ISSN1027-5495. Functional Materials, 31, No.4 (2024), p. 508-515
doi:http://dx.doi.org/10.15407/fm31.04.508

Effect of thermal spraying of different ceramic coatings on rotational fatigue life of AISI 1020 alloy

Saad Gh. Rifai, Edrees E. Khadeer

Department of Physics/ College of Science/ University of Mosul

Received July 25, 2024

The effect of thermal coating of AISI 1020 alloy substrate on the fatigue life during rotation was studied in comparison with the fatigue strength of the substrate. A rotating fatigue tester (HSM 19) was used to test the specimens at room temperature. Fatigue tests were carried out at various stress levels to obtain S-N curves. Two coatings were applied to the AISI 1020 steel alloy using thermal spraying method: a NiAlCrSi bonding coating and a thermal barrier coating based on an alloy (Al_2O_3+MgO). The microstructure and phase composition of the coatings were investigated using SEM and XRD methods. Compositional analysis revealed the presence of numerous precipitates and primary phases, including Al_2O_3, Cr_2O_3, and $CrNiO_4$, nickel or chromium secondary phases, as well as different oxides like $CrMgO_4$. The morphological results also show that the coating was quite heterogeneous, with a significant concentration of oxide inclusions, pores and microcracks. The fatigue strength results show that all coated alloys have reduced strength compared with the uncoated base alloy, which gradually decreases with increasing loads applied to them. It was also discovered that the alloy A_4, which contains a high weight fraction of Al_2O_3, was closest to the base alloy and showed the greatest improvement in fatigue compared to the other alloys.

Keywords: thermal spraying, ceramic powders, rotational fatigue, steel alloy AISI1020, bond coat, thermal barrier coating, ni-al cr si powder, Al_2O_3+MgO powder.

Вплив термічного покриття на втомну довговічність при обертанні сплаву підкладки AISI 1020. *Saad Gh. Rifai, Edrees E. Khadeer*

Вплив термічного покриття підкладки зі сплаву AISI 1020 на втомну довговічність під час обертання досліджували в порівнянні з втомною міцністю підкладки. Для випробування зразків, яке проводилося при кімнатній температурі, використовувався тип втомного пристрою, що обертається (HSM 19). Випробування на втому вимірювалися за різних рівнів напружень для отримання кривих S-N. Два покриття були нанесені методом термічного розпилення на сталевий сплав AISI 1020: NiAlCrSi як сполучне покриття та термобар'єрне покриття на основі сплаву (Al_2O_3+MgO). Мікроструктура покриття та фазовий склад були досліджені за допомогою методів SEM та XRD. Склад зразків виявив наявність численних осадів та первинних фаз, включаючи Al_2O_3, Cr_2O_3 та $CrNiO_4$, вторинних фаз нікелю або хрому, а також різних оксидів, таких як $CrMgO_4$. Морфологічні результати також показують, що покриття було досить неоднорідним, зі значною концентрацією включень оксиду, пор та мікротріщин. Результати міцності втоми показують, що весь покритий сплав мав зменшену міцність в порівнянні з непокритим базовим сплавом, яка поступово зменшувалася зі збільшенням доданих до нього навантажень. Було також виявлено, що сплав (A_4), який містить високу вагову частку Al_2O_3, був найближчим до базового сплаву і показав найбільше поліпшення міцності втоми порівняно з іншими сплавами.

1. Introduction

Thermal spraying is a technology widely used to apply ceramic and other coatings to highly stressed structural components, including equipment for the aerospace industry, energy industry, and aerospace applications where high abrasion, corrosion, and heat resistance are required [1]. This technology is widely used in many industrial applications as an alternative to hard chrome plating and overlay coating techniques. The use of the appropriate coating can increase the life of components and reduce the risk of failure, which also results in lower long-term maintenance costs [2]. However, in existing and new industrial applications, the performance of thermally sprayed components depends not only on the choice of coating materials, deposition process parameters, but also on a number of other design factors such as operating conditions, coating thickness, work classes and substrate properties [3].

The fatigue behavior of coated components needs to be clarified as there is little information available on the specific system. There is still very little information available on the mechanisms of fatigue or fatigue failure of coated systems. There are studies [4, 5] devoted to the comparison of factors influencing the fatigue behavior of coatings such as CoNiCrAlY, NiCrBSi and WC-Co. Most studies generally agree that the application of thermal spray coatings deteriorates the fatigue strength of the entire system, but there are also studies indicating that a small percentage of coatings can increase the fatigue properties [6]. Recent studies show that fatigue properties are very sensitive to changes in deposition process parameters [7]. Understanding crack formation mechanisms is crucial to optimizing the basic parameters of the spraying process. It is known from previous studies [8] that fatigue crack formation occurs due to different mechanisms (corrosion, lamination failure of the base material, and peeling). Under cyclic loading, these mechanisms are mutually combined, and the resulting destruction of the coating can be caused by either one mechanism or a combination of several of them. Factors such as coating thickness, substrate material, spray conditions, and substrate properties prior to coating application have the greatest influence on the fatigue behavior of the resulting system. As we mentioned previously, fatigue properties are affected by many factors, be it pre-spray or spray parameters, as well as post-spray treatment. Evaluation of individual process parameters in relation to the resulting fatigue properties of the overlaid system is essential for a deeper understanding of fatigue fracture mechanisms. Another factor that affects fatigue properties is the residual stress present in both the substrate and the thermally sprayed coatings [8]. The current problem is the lack of publicly available information that comprehensively describes this issue [8]. However, over the past few years, the number of studies devoted to the influence of various deposition agents on the fatigue behavior of thermally sprayed parts has increased significantly [9]. From the above information, it is clear that these failure mechanisms are interconnected and actively interact. The degree of their occurrence depends on their combined variables, which makes it impossible to fully optimize the spraying process for all types of limitations on fatigue mechanisms. The reason is that a change in one parameter and the subsequent increase in resistance to a specific failure mechanism lead to a decrease in resistance to other failure mechanisms. For this reason, it is important that the thermal spraying process is optimized against fatigue fracture taking into account all types of failure mechanisms and is considered as a compromise solution corresponding to the desired final properties [10].

The purpose of the study was to obtain new results that could be compared with other studies. The increased requirements for operating temperatures are due to the future use of these coatings in the energy industry.

2. Experimental

2.1 Material Selection

Mild steel alloy A_s was chosen as a base material because it will be used in finished parts in the energy industry. Its chemical composition is given in Table 1.

Table 2 shows the percentages of ceramic powders used for bond and thermal barrier coatings.

2.2 Fatigue Machining Test Specimen

The fatigue test specimens were manufactured according to the standard specifications of the fatigue testing apparatus used in this work (HSM 19).

2.3 Thermal Spraying

The sample surface preparation before spraying is very important for the success of

Table 1. Chemical composition of AISI 1020 alloy

Chemical composition, wt. %							Sample code	Element
S	Ni	Cr	C	Si	Mn	Fe		
0.061	0.02	0.08	0.04	0.16	0.62	Balance	Ao	Wt. %

Table 2. Weight Percentages of Powders Coating

Powder Name	Chemical formula	Sample code	Chemical composition, wt. %			
			Ni	Cr	Al	Si
Bond Coating (BC)	NiCrAlSi	A1	57	31	11	1

Powder Name	Chemical Formula	Sample Code	Chemical composition, wt. %	
			Al_2O_3	MgO
Thermal Barrier Coating (TBC)	$MgO+Al_2O_3$	A_2	25	75
		A_3	50	50
		A_4	75	25
		A_5	100	0
		A_6	0	100

Table 3. The Flame Thermal Spraying Process Parameters

Oxy – Acetylene Mixing	4: 0.7
Flame Spray Temp	3000°C
Powder feeding (g/min)	3.5
Spraying Distance	14 cm
Particle size of Powders	25 – 75 μm
Coating Time	20 to 40 s
Maximum Thickness Coating	170 μm

the coating process because the degree of adhesion of the coating to the substrate surface depends on the mechanical interlocking of the coating molecules and the substrate surface. After cutting and smoothing the samples as we mentioned previously, their surface was roughened using silicon carbide paper with a fineness grade of 220#; then it was washed and cleaned by ultrasound with an acetone solution for (300 seconds) to remove grease and other contaminants from the surface. The samples are then washed with distilled water, dried quickly with hot air, and placed in sealed bags until the coating process is carried out. The ceramic coatings were obtained using a Chinese-made QH-2/H jet welding torch.

The mixing ratio of oxygen with acetylene can be determined through a special regulator (flowmeter). A special clamp is designed to hold the spray gun fixed at a spraying distance of 14 cm towards the rotating electric base to hold the samples. Table 3 shows other factors related to the thermal spraying process.

It was also necessary to maintain the substrate temperature between (200-400°C) before spraying to avoid delamination during the final cooling.

2.4 Fatigue Testing Machine

The rotary bending fatigue testing machine (HSM 19 HITECH) shown in Fig. 1 was used to carry out constant and variable capacity fatigue tests. This device operates at a frequency 2800 rpm, which imposes cyclic bending stress in a sine wave manner with constant amplitude and zero mean stress. The value of the stress ratio is (R = –1). The load is applied perpendicular to the axis of the sample, resulting in a bending moment, and thus the surface of the sample will be subjected to tension and compressive stresses when it rotates. The load required for a given stress magnitude can be determined by considering the specimen as a cantilever beam, as shown in the following expression [20]:

$$\sigma = \frac{125.7 \cdot 32P}{\pi \cdot d^3} \quad (1)$$

Where P is the load required to be applied for a given stress (σ), and d represents the minimum

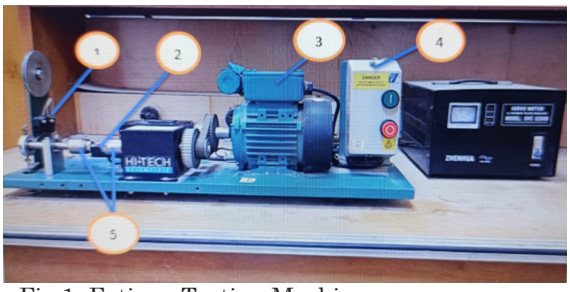

Fig.1: Fatigue Testing Machine

diameter of the specimen measured in mm. The distance from this point to the line of action of the applied load is 125.7 mm. The device is equipped with a counter to count the number of cycles until the specimen fails. This meter has a small switch that automatically stops it when the specimen is broken. The test specimen is clamped between two grips in the drilling rig as shown in Fig. 1, where (1) is the circuit breaker, (2) is the fatigue test specimen, (3) is the electric motor, (4) is the power unit, and (5) is a jaw rig. At least two specimens were used to plot the SN curves for each group.

2.5 Microstructure and Phase Analysis

XRD analysis was used to identify the phase composition of the bond and thermal barrier layers using a Shimadzu Company XRD 6000 instrument at the Nanotechnology Center/University of Technology. The microstructure of the coating layer was studied by scanning electron microscopy (SEM) with energy dispersive X-ray spectroscopy (EDX) of the coated sample by an Inspector S50 device in the laboratories of the Nanotechnology Center/University of Technology. Cross-sections of the fracture specimens were examined using an optical microscope (OM) (Hamilton) equipped with an imaging camera for examination purposes.

3. Results and Discussion

3.1 X-ray Diffraction Examination

As shown in Fig. 2, the X-ray diffraction (XRD(patterns of all sprayed coatings confirmed the presence of dominant compounds such as Cr_2O_3 and $CrNiO_4$, in addition to the aluminum oxide phase Al_2O_3. Results also indicated the presence of some weak peaks, which appear as precipitates of many secondary phases.

3.2 Scanning Electron Microscope Examination

The surface morphology of the bonding coating A_1 examined using a scanning electron microscope, as shown in Fig. 3, revealed a scatter of coating components over the cross-section of

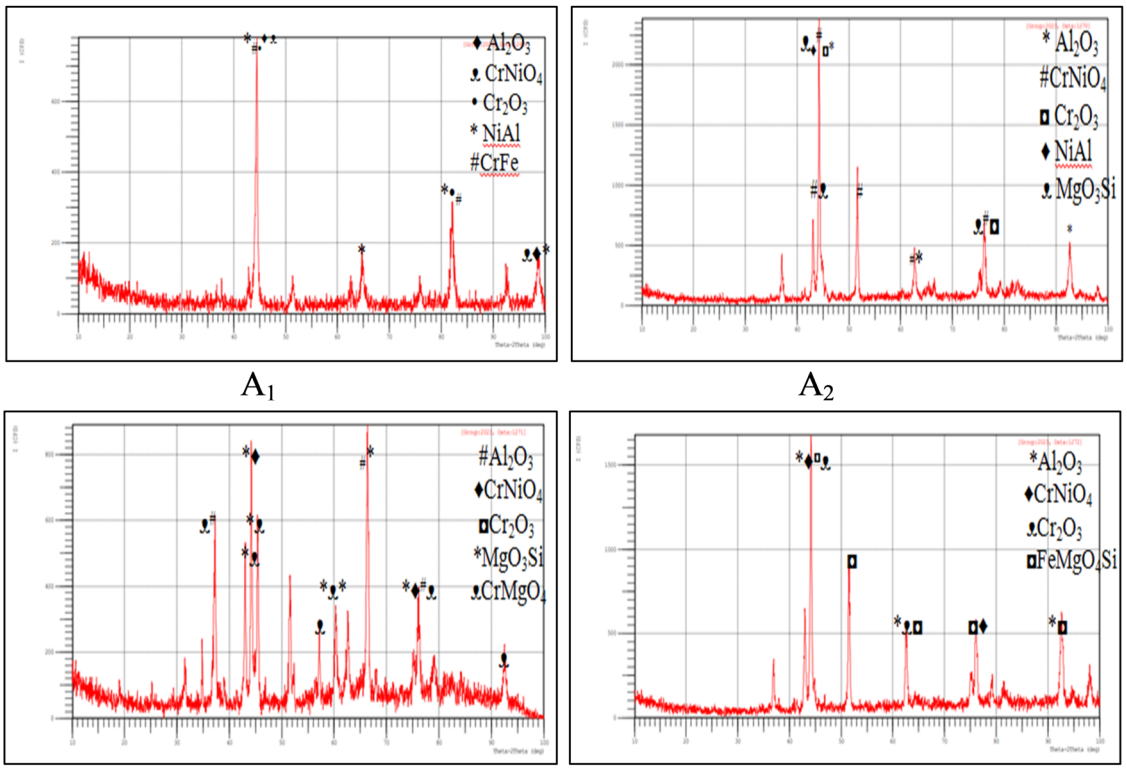

Fig. 2: X-ray diffraction patterns of coated r specimen

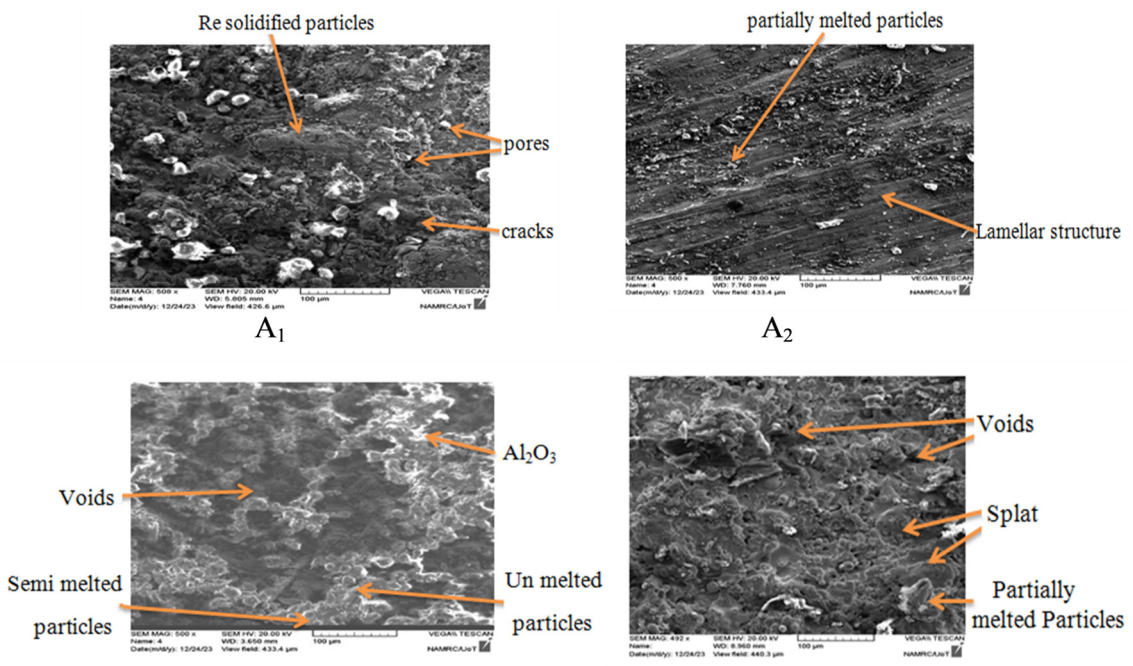

Fig. 3: Surface cross-section of coated alloys

the alloy and agglomerations in other places. This leads to the appearance of low- and high-density areas in microscopic observations [11]. It was also found that there are also surface defects such as partially dissolved particles, pores, and voids in the microstructure of the coated alloy.

Microscopic examinations of the A_2 coating layer show lamellar surface structure occurring as a result of the gradual cooling process of coating particles when they collide with the alloy surface. The surface also contained microcracks, some partially melted particles which are believed to belong to aluminum (Al_2O_3) or chromium (Cr_2O_3) oxides and do not have sufficient time to dissolve during the spraying process due to the high flow speed of the powder during the spraying process [12]. As for the surface coating (A3), it can be seen that the surface consists of interconnected particles with an irregular structure, which leads to the formation of voids. These gaps were formed after some powder particles were destroyed during the spraying process [13, 14]. Pores, semi-particles, and some undissolved particles were also observed in the microscopic structure of A4 coatings. A distinctive feature of the coating A4 from others is the presence of spots, which sometimes reach a micrometer in size and may be larger. This is the result of the remelting and solidification of the coating powder after it hits the alloy surface [15].

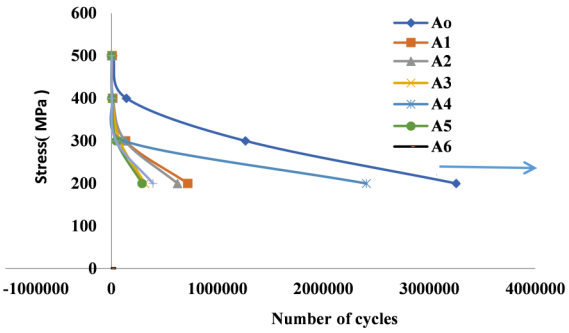

Fig. 4: Wöhler curves of coated and uncoated steel alloy

3.3 Rotating Fatigue Examination

Fig. 4 illustrates the Wöhler or (S-N) curves of the coated and uncoated (AISI 1020) steel, which represent the relationship between stresses and the number of cycles to failure. The test was carried out using loads in the range from 10 to 25 N. The resulting stresses were calculated using equation (1), as shown in Table 4. Also, the fatigue limit σ_L of the uncoated steel was found from the curve, which is equal to 200 MPa.

Rotating fatigue results showed that the number of cycles to failure for all samples gradually decreased with increasing applied stress. It was also noted that alloy coatings with different mass fractions of alumina and magnesia powders reduce the fatigue strength of the base. This is due to the fact that these powders led to

Table 4: Stress values and number of cycles to failure for the uncoated alloy

Fatigue Limit (σL) (MPa)	Number of Average Cycles to Failure	Applied Stress (σ) (MPa)	Load (N)
200	> 3254871	200	10
	1265487	300	15
	141798	400	20
	12683	500	25

the rapid formation and propagation of microscopic cracks in the coatings when exposed to cyclic stresses (tension and compression) during the testing period.

Regarding the rotational fatigue resistance of A_2, A_3, A_5, and A_6 coatings, we find that they were rapidly destroyed during the fatigue test, so it can be said that their fatigue behavior was similar with changing stress level (200-500 MPa).

By comparing these alloys with each other, we find that the alloy coated by A_2 showed the best result compared to the A_3, A_5, A_6 coating alloys, so that the average number of fatigue cycles was 623641 at stress of 200 MPa. This is the highest value compared to the other alloys mentioned, but the coating A_2 could not withstand the increase in stress and failed when the stress level reached 500 MPa, at a cycle number of 637. Other alloys had lower fatigue life; thus, for sample A_5 the average number of fatigue cycles to failure was 289513 cycles at a stress of 200 MPa, and it underwent rapid failure at the number of cycles 420 when the stress was increased to 500 MPa. The reduction in fatigue life of these alloys is due to many factors, including the formation of undesirable secondary phases or the large number of defects in the coating layer, such as pores, microscopic cracks, or voids, which are some of the most important centers of internal stress concentration during testing and lead to cracking and stretching of the coating layer. The crack inside the alloy weakens its resistance to fatigue [16]. It was also found that the alloy coating A_4, although not as good in performance as the base alloy, was closest to the performance of the uncoated base alloy. It was ideal compared to the bond coating alloy and other coating alloys.

To understand how the applied stresses affect the fatigue behavior of the tested samples, in addition to identifying the crack initiation and propagation sites, the fracture region after specimen failure was examined using a conventional optical microscope. Fig. 5 shows the overall fatigue failure surface of a specimen tested at 300 MPa.

Examination of the fracture surface of the A_o specimen showed that the onset of fracture was not clear, and the growth of microscopic cracks occurred from the surface and spread deep into the alloy in all directions. The voids observed in Fig. 5a are associated with the propagation of fatigue cracks throughout the base material. This gives the uncoated steel a characteristic cup-and-cone fracture. A random herringbone pattern was also observed within the alloy before its failure, which is typical for viscous fractures [17].

The optical microscopy results show that both the base steel alloy A_o and the coating alloy A_5 have significant difference in fracture cross-section. The largest smooth, polished area characteristic of brittle fracture is observed. This is due to the fact that the surface groove formed by the coating alloy as a result of the thermal spraying process caused higher stress concentration at high temperatures and led to faster failure [18]. According to L. O. A. Affonso [19], stress concentration on the surface results in faster propagation of the cracks close to it. This will cause it to fracture faster than the base specimen. The faster fracture resulted in a smaller fatigue crack region and a larger final fracture region.

Returning to Fig. 5, for the samples of A_1, A_2, and A_3, we find that the fractured surface is characterized by peeling off of the coating layer to a very large extent. This indicates that these coatings cannot withstand fatigue stresses (tension and compression) that occur when a vertical load is applied to the sample. In addition, the difference in expansion coefficients between the base alloy and the coating can lead to failure of the coating and its separation from the alloy, thereby reducing the fatigue life of these alloys [20].

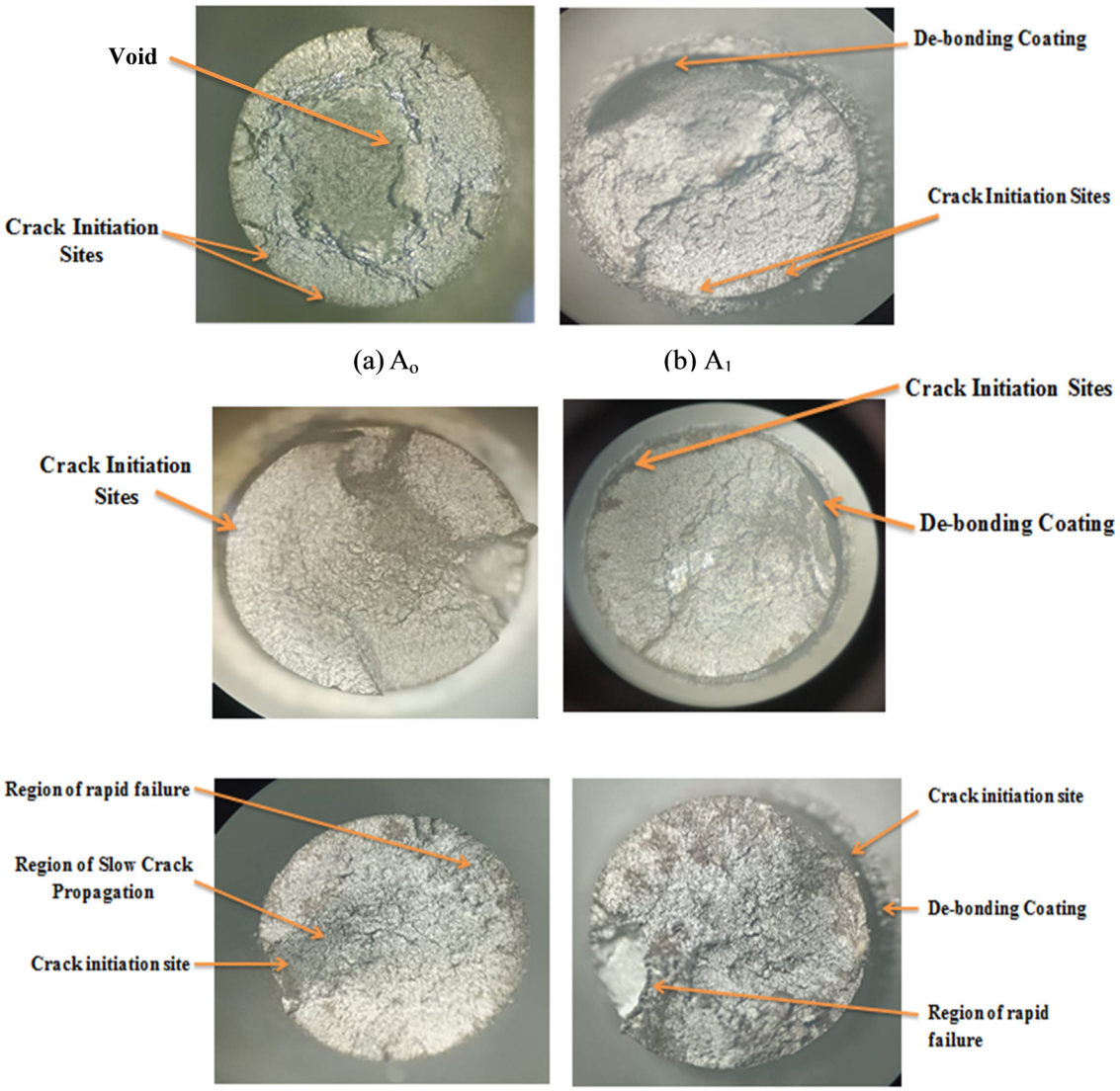

Fig. 5: Cross-sections of fractures of coatings made of different alloys (40X)

The fracture surface of the A_4 alloy coating tested at 200MPa with 2495480 cycles to fracture, shown in Fig. 5e, gives us a clear idea of the performance of this alloy. The fracture region can be divided into three parts. The crack initiation zone is located near the periphery of the sample, from which the crack slowly propagates across the entire cross-section of the sample, leaving behind a relatively smooth surface and a dark color image (propagation zone). Also at 180° from the initiation zone, one can see a relatively rough surface and groove-like traces that correspond to the viscous fracture zone.

4. Conclusions

1. The main objective of this research is to examine the fatigue behavior of the AISI 1020 steel alloy coated by two types of coatings (NiCrAlASi) and Al_2O_3, with different weight fractions.

2. Microstructure analysis revealed the presence of Al_2O_3, Cr_2O_3, and $CrNiO_4$ phases as main phases, as well as phases like CrFe and $CrMgO_4$ in the form of secondary precipitations.

3. The SEM study showed that the thermal coatings were very heterogeneous, with a high concentration of oxide inclusions, pores, microcracks, and voids.

4. All coated alloys exhibited lower rotational fatigue resistance than the base alloy, which gradually decreased with increasing stresses.

5. Rotational fatigue experiments on A_1, A_2, A_3, A_5, and A_6 samples revealed rapid failure at stress levels between 200 and 500 MPa.

6. The results also showed that although the A_4 sample was subjected to gradual fatigue failure, the fatigue resistance behavior of this specimen was the best in comparison with the rest of the coated alloys, and it was most similar to the base alloy.

7. The thermal spray method for coating alloys is cost-effective and takes less than half a minute.

Acknowledgment

The researchers sincerely thank the University of Mosul/College of Science for providing monetary assistance and all possible facilities to achieve the results of this research.

References

1. A. Mazin, A. Mahmood, C.E. Gader, *Oxidation Communications*, **45**(1), 2022.
2. Saad Gh. Rifai, Edrees E. Khadeer. *J. Engin. Res. Rev.*, **1**(1), 51, 2024.
3. Mcgrann, R.T.R., Greving, D.J., Shadley, J.R., Rybicki, E.F., Kruecke, Tl.T., Bodger, B.E. *Surface coating technology*, **59**, 108, 1998.
4. Osawa, S., Itsukaichi, T., & Ahmed, R., *J. Thermal Spray Technology*, **14**, 495, 2005.
5. Voorwald, H. J. C., Souza, R. C., Pigatin, W. L., & Cioffi, M. O. H., *Surface and Coatings Technology*, 190(2-3), 155, 2005.
6. Tipton, A., The Effect of HVOF Thermal Spray on the Elevated Temperature High Cycle Fatigue Behavior of a Martensitic Stainless Steel. Dresser-Rand, New York, NY., 2002
7. La Barbera-Sosa, J. G., Santana, Y. Y., Villalobos-Gutiérrez, C., Cabello-Sequera, S., Staia, M. H., & Puchi-Cabrera, E. S., *Surface and Coatings Technology*, **205**(4), 1137, 2010.
8. Ahmed, R., & Hadfield, M., *J. Thermal Spray Technology*, 11, 333, 2002.
9. Al-Fadhli, H.Y., Stokkes, J., Hashmi, M.S.J., Yillbas, B.S., *Surface and Coatings Technology*, **200**, 2006.
10. Alloys, Electrical Resistance. *Special-Purpose Materials*. 1998.
11. Ahmed, B. S., & Jassim, I. K., *J. University of Babylon for Pure and Applied Sciences*, **27**(4), 98, 2019.
12. Michalak, M., Sokołowski, P., Szala, M., Walczak, M., Łatka, L., Toma, F. L., & Björklund, S., *Coatings*, **11**(8), 879, 2021.
13. Rana, N., Mahapatra, M. M., Jayaganthan, R., & Prakash, S.,. *J. Alloys and Compounds*, **615**, 779, 2014.
14. Chatha, S. S., Sidhu, H. S., & Sidhu, B. S., *Surface and Coatings Technology*, **206**(19-20), 3839, 2012.
15. Callister Jr, W. D., & Rethwisch, D. G., Fundamentals of materials science and engineering: an integrated approach. John Wiley & Sons , 2020.
16. Puntambekar , G.S.Grewal , P.BJoshi and Sampathkumaran. *International Journal of Latest Research in Science and Technology*, pp.132U, N.-137, 2014.
17. Alweendo, S. T., Morita, M., Hasegawa, K., & Motoda, S. *Materials*, **14**(23), 7480, 2021.
18. Ahmed, R. & Hadfield, M. *J. Thermal Spray Technology*, 11(3), 333, 2002.
19. Affonso, Luiz Octavio Amaral. Machinery Failure Analysis Handbook. Gulf Publishing Company, 2013.
20. Ana Isabel García-Diez, Juan José Galán-Díaz, Manuel Ángel Graña-López, and Mar Toledano-Prados. *Applied Science*, **12**, 2369, 2, 2022.